

# Dissociation spectrum of $\text{H}_2^+$ from a short, intense infrared laser pulse: vibration structure and focal volume effects

Liang-You Peng, I D Williams and J F McCann

International Research Centre for Experimental Physics

School of Mathematics and Physics,

Queen's University Belfast,

Belfast BT7 1NN, Northern Ireland, UK.

email : l.peng@qub.ac.uk

**Abstract.** The dissociation spectrum of the hydrogen molecular ion by short intense pulses of infrared light is calculated. The time-dependent Schrödinger equation is discretized and integrated in position and momentum space. For few-cycle pulses one can resolve vibrational structure that commonly arises in the experimental preparation of the molecular ion from the neutral molecule. We calculate the corresponding energy spectrum and analyze the dependence on the pulse time-delay, pulse length, and intensity of the laser for  $\lambda \sim 790\text{nm}$ . We conclude that the proton spectrum is a both a sensitive probe of the vibrational dynamics and the laser pulse. Finally we compare our results with recent measurements of the proton spectrum for 55 fs pulses using a Ti:Sapphire laser ( $\lambda \sim 790\text{nm}$ ). Integrating over the laser focal volume, for the intensity  $I \sim 3 \times 10^{15}\text{W cm}^{-2}$ , we find our results are in excellent agreement with these experiments.

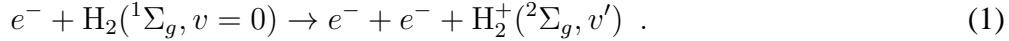
*To be submitted to J. Phys. B*

## 1. Introduction

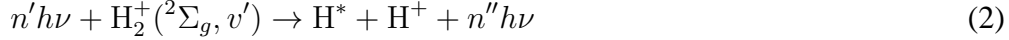
Energy transfer mechanisms in molecules exposed to short intense laser pulses is of great current interest [1]. Processes such as multiple photoionization, multiphoton dissociation and high-order harmonic generation have been studied for a wide-range of molecular species and an excellent up-to-date review of the field has been provided by Posthumus [2]. The hydrogen molecule and molecular ion represent ideal systems for a detailed understanding of ionization and dissociation dynamics of small molecules [3]. The simplicity of molecule means that it is the system of choice for theoretical studies. In general the mechanisms of dissociation [4] and ionization [20, 16, 17] are very well characterised for this molecule. Nonetheless, the solution of three-body disintegration, incorporating spatial and temporal variations in the laser pulse as well as the thermal ensemble of molecular states, remains a severe challenge for simulation. Consequently, progress has been fairly limited in dissociative ionization spectrum calculations.

Although there exists a wealth of data on the photofragment energy spectrum for the neutral molecule,  $\text{H}_2$ , and its deuterated forms [2]. the data for the much simpler isolated

molecular ion is extremely scarce. The feasibility of experimental studies is hampered by the difficulty in preparing the molecular ion. In fact experiments on  $H_2^+$  in intense laser fields has only become possible in the last 4 years [10, 11, 12, 13] due to refinements in ion sources and charged molecular beam spectroscopy. Typically a small portion of the molecules, at a temperature of a few hundred Kelvin and hence predominantly in the vibrational state ( $v = 0$ ), can be converted into the bound molecular ion by electron-impact ionization,



The molecular ions can be extracted, cooled and collimated into a beam that can be injected to the focus of the laser. The photodissociation and/or photoionization processes,



produce ions and electrons that can be collected and analysed. Owing to the small nuclear mass, the expansion (vibration) is very rapid - on the scale of 10 fs or less. Consequently the molecule relaxes extremely rapidly on the timescale of the pulse rise time. The design of infrared pulses that would, among other things, allow the resolution of timescale of a fraction of a femtosecond.

The main aim of this paper is a direct comparison of theory and experiment for the proton energy spectrum produced by a short intense infrared pulse interacting with  $H_2^+$  [10, 12]. Fragment-ion coincidence measurements that isolate the dissociation and dissociative ionization processes and make the comparison of theory and experiment feasible and realistic. The molecular dissociation dynamics are modelled using a two-state approximation and takes account of the laser pulse profile. Although this approach neglects the ionization channels, the results for dissociation energies are in excellent agreement with the observations.

## 2. The model

### 2.1. Physical considerations

The characteristic vibrational and rotational time of the  $H_2^+$  molecule are  $T_{\text{vib}} \sim 15$  fs and  $T_{\text{rot}} \sim 170$  fs, respectively. For a pulse duration 60 fs or less, the laser interaction is sudden on the rotational timescale. Thus one can assume a random statistical orientation of the molecular axis, and that the nuclei recoil along the axial direction. We assume that the bound ion is created by vertical transitions from the  $v = 0$  state of the neutral  $H_2(X^1\Sigma_g)$ . The parameters of this potential surface are, bond length  $R_0 = 1.40$ a.u. with vibrational constants,  $\hbar\omega_0 = 0.546$ eV and  $x_e = 0.0276$ . The  $v = 0$  wavepacket is promoted onto the corresponding molecular-ion surface  $H_2^+(X^2\Sigma_g)$  with parameters  $R'_0 = 2$ a.u.,  $D'_0 = 2.65$ eV,  $\hbar\omega' = 0.288$ eV and  $x'_e = 0.0285$  [41]. The  $v = 0$  state is projected onto the  $v'$  manifold of states according to the Franck-Condon principle [34]. The manifold of  $v'$ -states is then subjected to intense Ti:Sapphire light.

In the dissociation process, momentum is conserved, for a symmetric pulse, and the recoiling atom and ion have equal and opposite velocity in the centre-of-mass frame. The ions and atoms are collected in coincidence such that dissociation and dissociative ionization can

be discriminated. However, depending on the method of measurement, the atomic fragments can arise from the entire focal volume of the laser. So a valid theoretical comparison must firstly establish the single molecule energy spectra, and then sum these spectra with the appropriate focal volume weighting for the experiment. The intensity  $I_0(\rho, z)$  of a focused cylindrically-symmetric laser beam is spatially Gaussian in the radial  $r$ -direction and Lorentzian along the axis  $z$  [1]

$$I_0(\rho, z) = \frac{I_f}{1 + (z/z_R)^2} \exp \left\{ \frac{-2\rho^2}{w_0^2 [1 + (z/z_R)^2]} \right\}. \quad (3)$$

where the minimum waist of the beam  $w_0$  and Rayleigh range  $z_R$  are given by

$$w_0 = \frac{2f\lambda}{\pi D}, \quad \text{and} \quad z_R = \frac{\pi w_0^2}{\lambda} \quad (4)$$

respectively. In our method, we first discuss the single-molecule response in detail, and then describe the orientation-averaged and focal-volume integrated results.

The electronic coordinate, with respect to the origin at the internuclear midpoint, is denoted by  $\mathbf{r}$  and the internuclear coordinate is written as  $R$ . The two lowest electronic states, namely the ground state  $X^2\Sigma_g^+$  ( $\phi_g$ ), and  $A^2\Sigma_u^+$  ( $\phi_u$ ) are sufficient for the study of pure dissociation dynamics. The corresponding adiabatic energies are  $E_g(R)$  and  $E_u(R)$ . Then the two-state approximation is

$$\Psi(\mathbf{r}, R, t) = F_g(R, t)\phi_g(\mathbf{r}, R) + F_u(R, t)\phi_u(\mathbf{r}, R) \quad (5)$$

where  $F_g(R, t)$  and  $F_u(R, t)$  are the time-dependent nuclear wavefunctions. In restricting the electronic spectrum to the two lowest levels, the calculations will inevitably be gauge dependence. For low frequency fields (much less than the energy level gap) it is essential to use the length gauge for the laser-molecule interaction. Let us take the light as linearly polarized along the direction  $\boldsymbol{\varepsilon}$ , and denote the dipole moment between  $\phi_{u,g}$  as  $\mu(R)$ . Writing the electric field as  $\mathbf{E}(t)$ , the coupling potential is denoted by  $V_L(R, t) = -\mu(R)\mathbf{E}(t)u$ , where  $u \equiv \boldsymbol{\varepsilon} \cdot \hat{\mathbf{R}}$ . Within the axial-recoil approximation,  $\theta_k = \cos^{-1} u$ , is the angle of ejection of the ion(atom) with respect to the polarization vector. Averaging over the molecular orientation is equivalent to averaging the projection of the electric field along the molecular axis. Since the dissociation rate increases rapidly with intensity over the range,  $I \sim 10^{12} - 10^{14} \text{ W cm}^{-2}$ , it follows that the atoms and ions are ejected predominantly along the polarization direction. It is highly anisotropic. However at the higher intensities,  $I \sim 10^{15} \text{ W cm}^{-2}$ , the dissociation process begins to saturate and, as we will show, the angular distribution is broader.

## 2.2. Numerical method

Taking  $m = \frac{1}{2}m_p$  to denote the reduced mass of the protons, and using atomic units, the two-state coupled equations are:

$$i\frac{\partial}{\partial t}F_g(R, t) = -\frac{1}{2m}\frac{\partial^2}{\partial R^2}F_g(R, t) + E_g(R)F_g(R, t) + V_L(R, t)F_u(R, t), \quad (6a)$$

$$i\frac{\partial}{\partial t}F_u(R, t) = -\frac{1}{2m}\frac{\partial^2}{\partial R^2}F_u(R, t) + E_u(R)F_u(R, t) + V_L(R, t)F_g(R, t), \quad (6b)$$

To a very good approximation [25] the potential functions can be written in the form,

$$E_g(R) = 0.1025 [e^{-1.44(R-2)} - 2e^{-0.72(R-2)}], \quad (7)$$

$$E_u(R) = 0.1025 [e^{-1.44(R-2)} + 2.22e^{-0.72(R-2)}] \quad (8)$$

Similarly, the dipole moment [26] can be fitted by the function [27]

$$\mu(R) = -\frac{1}{(2 + 1.4R)} + \frac{R}{2\sqrt{1 - p^2}} \quad (9)$$

with,  $p = (1 + R + R^2/3)e^{-R}$ . For a frequency  $\omega_L$  and peak field strength  $E_0$ . This is related to the cycle-average intensity,  $I = \frac{1}{2}c\varepsilon_0 E_0^2$ . The time-dependence of the field can be written explicitly as

$$E(t) = E_0 f(t) \cos \omega_L t \quad (10)$$

In this paper we use the Gaussian profile that most closely models the pulses in the experiment of interest,

$$f(t) = \exp \left[ -(4 \ln 2) \left( \frac{t - T_c}{T_p} \right)^2 \right] \quad (11)$$

where  $f(T_c) = 1$  is the maximum, and  $T_p$  defines the duration of the laser pulse.

### 2.3. The grids

Discretization methods previously developed for photodissociation [32] and photoionization of molecules [19, 16, 17] can be readily applied. The discrete-variable representation (DVR) has proven to be a very efficient and accurate method in solving both time-independent and time-dependent Schrödinger equations. The Cartesian Lagrange functions [29] are given by

$$\begin{aligned} f_i(x) &= \sum_k \varphi_k^*(x_i) \varphi_k(x) \\ &= \frac{1}{N} \sum_k \exp \left[ -i \frac{2\pi k}{N} x_i \right] \exp \left[ i \frac{2\pi k}{N} x \right] \end{aligned} \quad (12)$$

with the mesh points  $x_i = i - (N + 1)/2$  ( $i = 1, 2, \dots, N$ ). The radial coordinate  $R$  is discretised on this mesh Cartesian mesh between the limits  $R_{\min} \leq R_j \leq R_{\max}$ , with  $j \in \{1, 2, 3, \dots, N - 1, N\}$ , such that:

$$R_j = \frac{(R_{\max} - R_{\min})}{N - 1} [j - \frac{1}{2}(N + 1)] + \frac{1}{2}(R_{\max} + R_{\min}) \quad (13)$$

Then the wavefunctions are expanded as:

$$\begin{aligned} F_\sigma(R, t) &= \sum_{i=1}^N F_\sigma(R_i, t) f_i(R) \\ &= \frac{1}{N} \sum_{i=1}^N F_\sigma(R_i, t) \sum_{m=1}^N \exp \left[ i \frac{2\pi x_m}{N} \frac{(R - R_i)}{h} \right] \quad (\sigma = g, u) \end{aligned} \quad (14)$$

where  $h = (R_{max} - R_{min})/(N - 1)$ . Then the matrix equation corresponding to equations (6a and 6b) is a dense set of  $2N$  linear equations ( $\sigma = g, u$ ):

$$\sum_{j=1}^N T_{ij} F_{\sigma,j}(t) + \sum_{\tau,j} V_{\sigma\tau,ij}(t) F_{\tau,i}(t) = i \dot{F}_{\sigma,j}(t) \quad (15)$$

The matrix elements of the kinetic operator are given by [29]

$$T_{ij} = \begin{cases} \frac{\alpha\pi^2}{6} \left(1 - \frac{1}{N^2}\right) & i = j \\ (-1)^{i-j} \frac{\alpha\pi^2}{N^2} \frac{\cos[\pi(i-j)/N]}{\sin^2[\pi(i-j)/N]} & i \neq j. \end{cases} \quad (16)$$

where the scale factor is,  $\alpha = (N - 1)^2 m^{-1} (R_{max} - R_{min})^{-2}$ . The diagonal potentials are:

$$V_{uu,ij}(t) = \delta_{ij} E_u(R_j) \quad V_{gg,ij}(t) = \delta_{ij} E_g(R_j) \quad (17)$$

with the off-diagonal coupling:  $V_{ug,ij}(t) = V_{gu,ij}(t) = \delta_{ij} V_L(R_j, t)$ . We integrate the differential equations using the 18th order Arnoldi propagator as described by Peng et al [17].

As is well known [26], for  $R \rightarrow \infty$ , the moment  $\mu(R) \rightarrow \frac{1}{2}R$ , and the coupling is divergent in the molecular basis. This is simply a manifestation of the molecular basis and the use of the length gauge. It is necessary and convenient to transform to the asymptotic decoupled atomic eigenstates for the energy spectrum. These asymptotic states then evolve adiabatically at large distances and long times. However these states in turn are unbounded in configuration space. As shown by Keller [30], it is possible to project the diffuse adiabatic asymptotic states onto a compact momentum space. More importantly, this method produces the energy spectrum of the atoms that can be compared with experiment.

Following [28, 30] we divide the entire range of  $R$  into two regions; an internal region (*in*), where the molecular forces are significant, and an asymptotic region (*as*) where they are not. The short-range polarization potential means that the interaction region can be comparatively small (of the order 20 a.u.). Then the wavefunction can be partitioned as follows:

$$F_\sigma(R, t) = F_\sigma^{in}(R, t) + F_\sigma^{as}(R, t) \quad (18)$$

where:

$$\begin{aligned} F_\sigma^{as}(R, t) &= (1 - S(R)) F_\sigma(R, t) \\ F_\sigma^{in}(R, t) &= S(R) F_\sigma(R, t) \quad (\sigma = 1, 2). \end{aligned} \quad (19)$$

with

$$S(R) = \left(1 + \exp\left[\frac{R - R_s}{\tau_s}\right]\right)^{-1} \quad (20)$$

where  $R_s$  is dividing point and  $\tau_s$  is a parameter which determines the smoothness of the partition. In the asymptotic region Hamiltonian is diagonalised by transforming to the atom+ion states  $\chi_{1,2}$ :

$$\begin{pmatrix} \chi_1^{as}(R, t) \\ \chi_2^{as}(R, t) \end{pmatrix} = \frac{1}{\sqrt{2}} \begin{pmatrix} 1 & 1 \\ -1 & 1 \end{pmatrix} \begin{pmatrix} F_g^{as}(R, t) \\ F_u^{as}(R, t) \end{pmatrix}. \quad (21)$$

These states evolve into superpositions (sums over momentum) of the asymptotic states:

$$\chi_k^\pm(R, t, t') = \frac{1}{\sqrt{2\pi}} \exp \left[ i(k \mp \Delta(t, t'))R - i \frac{1}{2\mu} \int_{t'}^t d\tau [k \mp \Delta_0(t, \tau)]^2 \right] \quad (22)$$

where the ion quiver momentum is

$$\Delta_0(t, t') = \frac{1}{2} \int_{t'}^t d\tau' E(\tau') \quad (23)$$

A symmetric or zero-area pulse is such that:  $\Delta_0(+\infty, -\infty) = 0$ .

#### 2.4. Transformation to momentum space

The key step in obtaining an energy spectrum is the projection of the numerical wavefunction onto the the continuum of asymptotic states (22). It is efficient to do this by discretizing the  $k$ -space and performing a finite Fourier transform [30]. One difficulty with such an approach is that the momentum shift  $\Delta_0$  is a continuous function and inevitably leads to a mismatch of the  $k$ -grid. In the present calculations, we use the quadrature rule for the DVR to calculate the Fourier transform directly. We define the shifted Fourier transform:

$$\begin{aligned} \hat{\chi}_{1,2}(k \mp \Delta_0(t, t'), t) &= \frac{1}{\sqrt{2\pi}} \int_{R_{min}}^{R_{max}} e^{-i(k \mp \Delta_0(t, t'))R} \chi_{1,2}(R, t) dR \\ &= \frac{1}{N\sqrt{2\pi}} \sum_{i=1}^N \chi_{1,2}(R_i, t) \sum_{m=1}^N \frac{e^{-i[(k \mp \Delta_0(t, t')) - 2\pi x_m/Nh]}}{-i[(k \mp \Delta_0(t, t')) - 2\pi x_m/Nh]} \\ &\quad \times \left\{ \exp \left[ -iR_{max} \left( (k \mp \Delta_0(t, t')) - \frac{2\pi x_m}{Nh} \right) \right] \right. \\ &\quad \left. - \exp \left[ -iR_{min} \left( (k \mp \Delta_0(t, t')) - \frac{2\pi x_m}{Nh} \right) \right] \right\}. \end{aligned} \quad (24)$$

Although this quadrature is less efficient than the fast-Fourier transform, it allows for much greater flexibility in choosing the  $k$  and  $R$  grids.

At each time step, the projection onto the momentum space is made and the coherent momentum space wavefunction is calculated. This process is repeated and continued for some time after the end of the pulse. This allows the dissociating wavepacket still within the interaction region time to reach the asymptotic zone, and for the low energy components to be captured. Typically we extend the integration time to  $4T_c$  for this purpose. The  $k$ -space probability density is then given by [30]:

$$P_k(k) = \lim_{t \rightarrow \infty} |\hat{\chi}_1^{as}(k, t) + \hat{\chi}_2^{as}(k, t)|^2 \quad (25)$$

This choice of normalization gives:

$$P_d = \int_0^{+\infty} P_k(k) dk \quad (26)$$

is the total probability for dissociation. The dissociation energy is shared equally by the fragments so that the proton energy is given by  $E_p = (4m)^{-1}k^2$ . The energy spectral density can then be calculated from the equation:

$$P_E(E_p) = (dk/dE_p)P_k(k) = (m_p/k)P_k(k). \quad (27)$$

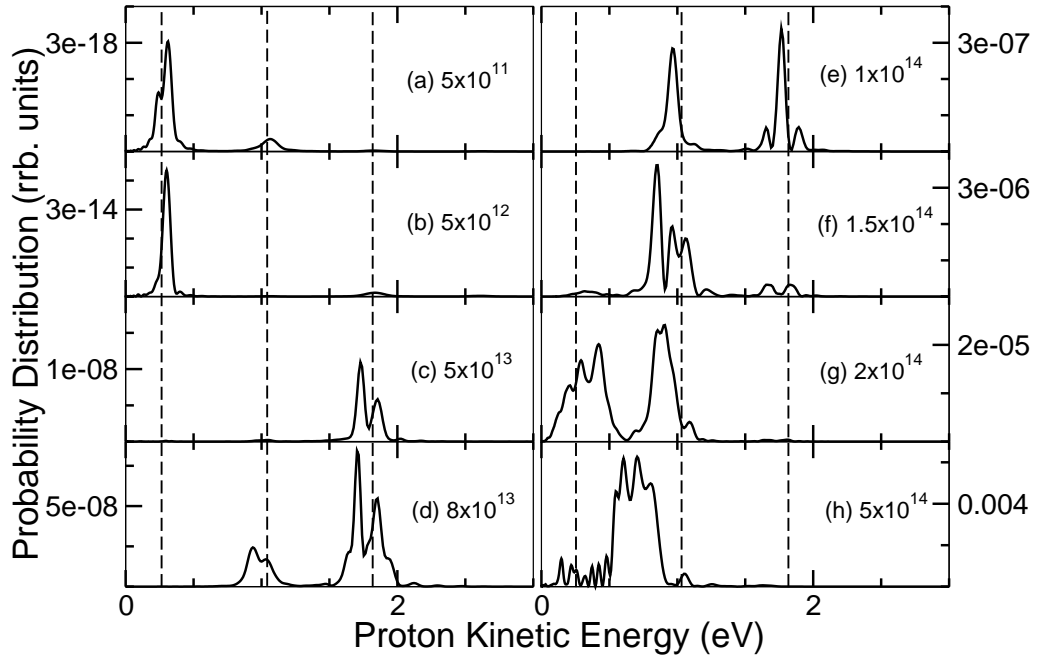


**Figure 1.** Proton energy spectrum  $P_E(E_p)$  for  $H_2^+(v' = 0)$  with  $\lambda = 790\text{nm}$  and pulse duration  $T_p = 55\text{fs}$ . The vertical lines indicate the anticipated energy of the two-photon, three-photon and four-photon absorption from  $v' = 0$ .

### 3. Results and discussion

#### 3.1. Dissociation from $H_2^+(v' = 0)$ at $\lambda = 790\text{nm}$

Firstly we consider photodissociation directly from  $v' = 0$  of  $H_2^+$ . There are several very accurate proton spectra calculation for  $v' = 0$  dissociation by  $\lambda \sim 330\text{nm}$  pulses for  $I \sim 10^{12} - 10^{14} \text{ W cm}^{-2}$  [6, 30]. We checked our calculations with these results and found excellent agreement in all cases. Now consider long-wavelength dissociation, we recall that the dissociation energy of the  $v' = 0$  state is  $D'_0 = 2.65 \text{ eV}$ . For  $\lambda \sim 790\text{nm}$ , corresponding to the Ti:Sapphire laser, the photon energy is 1.57 eV. Therefore dissociation is necessarily a second or higher order process. In figure 1 we present results for the proton energy spectrum  $P_E(E_p)$  for a  $T_p = 55\text{fs}$  pulse for a range of intensities. In these calculations, the number of points in  $R$ -space  $N = 512$  and the number of points in momentum space  $N_k = 2048$ , with  $R_{min} = 0.1 \text{ a.u.}$  and  $R_{max} = 28.5 \text{ a.u.}$ . For the splitting procedure we use,  $R_s \sim 0.7R_{max}$  and  $\tau_s = 0.2$ . For the time-dependent propagation we use  $\delta t = 0.01$ .

For a pulse of this length, the bandwidth (FWHM) is narrow  $\sim 0.03 \text{ eV}$ , and this is reflected in the sharply-defined proton energy (figures 1a, 1b and 1c) in the perturbation regime. In figure 1, the relative strength of the two-, three- and four-photon dissociation channels change dramatically with the variation of the pulse intensity. There is a propensity for the high-order process. As the interaction increases there is a leftward shift of the three-photon peaks in frame (e) to (g). This is due to the downwards Stark shift of the ground state. The leading-order term of this shift is approximately linear with intensity. The broadening of

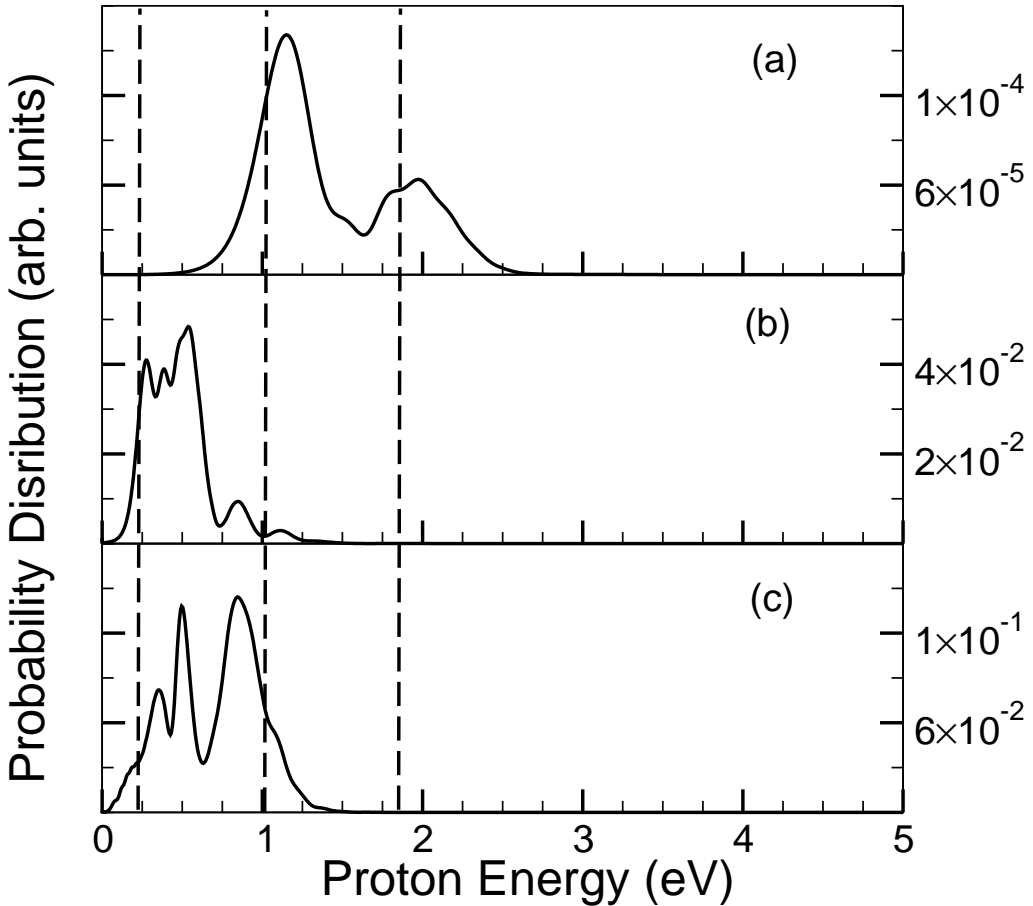


**Figure 2.** Proton energy spectrum  $P_E(E_p)$  for  $H_2^+(v' = 0)$  with  $\lambda = 790\text{nm}$  and  $I = 5.0 \times 10^{14} \text{W cm}^{-2}$ . The figure shows the effect of increasing pulse length (a).  $T_p = 5 \text{ fs}$ ; (b).  $T_p = 10 \text{ fs}$ ; (c).  $T_p = 20 \text{ fs}$ . The three vertical lines indicate the weak-field two-photon, three-photon and four-photon absorption energies.

the peaks is evidence of the mixing of vibrational levels and shortening of the lifetime of the decaying state  $v' = 0$ . In the last figure (h) at the highest intensity the spectrum is dominated by a large broad peak around 0.7 eV where the field-free vibrational structure is destroyed. At intensities above  $10^{15} \text{ W cm}^{-2}$ , the process is saturated by tunelling dissociation and the spectrum is dominated by low energy (less than 0.5 eV) protons [4]. This data underlines the difficulty in using time-independent perturbation theory to determine the ion spectrum and yield under these conditions.

The second calculation (figure 2) concentrates on the effect of pulse length for a fixed intensity  $I = 5 \times 10^{14} \text{ W cm}^{-2}$ . For pulses shorter than 15 fs the vibrational phase is accepted to play a role. However it is also important to note that the bandwidth has a significant effect. For example, a 5 fs pulse has a bandwidth of the order 0.35 eV. This would explain the skewness of the peak in figure 2(a), and the presence of the 4-photon peak. However, in figures 2(b) and 2(c), the results resemble the narrow-band data in figure 1. The oscillations in the peaks reflect wavepacket oscillations within the well and we discuss this in more detail later when investigating dissociation from excited vibrational states.

### 3.2. Dissociation from $H_2$ ( $v = 0$ ) at $\lambda = 790\text{nm}$

In the ion-beam experiments,  $H_2^+$  is prepared from the collisional ionization process (equation 1). The  $H_2$  ( $v = 0$ ) state is projected onto a coherent superposition of the  $H_2^+$  vibrational states,  $F_{v'}$ , where  $v' = 0, 1, \dots, 17$ . The amplitudes  $C_{v'}$  are given by the Franck-Condon factors. So that [34] in the absence of the laser the wavepacket evolves coherently

$$F_g(R, t') = e^{i\phi(t)} \sum_{v'=0}^{17} C_{v'} e^{i\phi_{v'} - iE_{v'} t'} F_{v'}(R) \quad (28)$$

where the relative phases  $\phi_{v'}$  are well defined constants, and  $E_{v'}$  are the vibrational energies. The overall phase  $\phi(t)$  depends on the time of formation of the ion. According to the Franck-Condon factors, the largest coefficients correspond to  $v' = 2, 3, 4$ . However a small fraction of the population will be above the dissociation limit leading to shake-off dissociation. Dunn's [34] estimate of this population was around 2.8%. In the present calculations, using the energy curves of equation (8), we obtain a value around 0.8%. In experiment the shake-off process is eliminated and plays no role. However, the coherence of the  $v'$  states has an important role. Since  $t' = 0$  is determined by the start of the pulse the molecules arrive in the focal volume with random vibrational phase. The random nature of the time delay is equivalent to averaging over random vibration phase. We can readily illustrate the physical consequences of this time delay in the proton spectrum. Suppose we choose the initial wavepacket as:

$$F_g(R, t' = 0) = F_{H_2}(v = 0, t = 0)$$

Then 0.8% of this wave function will naturally dissociate (shake-off) without laser interaction. In the calculations shown in 3, we present the proton energy distribution in the perturbation regime for a long pulse. The laser intensities are  $5 \times 10^9 \text{ W cm}^{-2}$  and  $5 \times 10^{10} \text{ W cm}^{-2}$  respectively, with  $\lambda = 790 \text{ nm}$  and pulse duration  $T_p = 55 \text{ fs}$ . The intensity-independent background that peaks at zero energy is the shake-off process. The rapid oscillations in this background are artifacts arising from the numerical method. The lowest energy states emerge most slowly and require long propagation times. The major source of noise is the splitting procedure that creates an interference pattern in the long-wavelength wavepacket components. However, above 0.3 eV the interference artifacts disappear and we are confident in the numerical accuracy of the energy spectrum in this range.

The 1-photon dissociation threshold means that only levels  $v' \geq 5$  appear. However the peak heights are modulated according to the values of both  $C_{v'}$  and the Franck-Condon dissociation factors. This vibrational structure has been resolved and measured experimentally [12, 13]. As predicted by the perturbation theory, the probability for the individual peak is proportional to the laser intensity. Very recently, Serov and coworkers [36] have obtained results of excellent agreement with these experimental measurements after careful consideration of averaging over initial ro-vibrational states and over the focus volume effect of the laser pulse.

In figure (4) the results for high intensity show dramatic differences with perturbation theory. In order to compare with experiment, it is desirable to eliminate the spurious shake-off

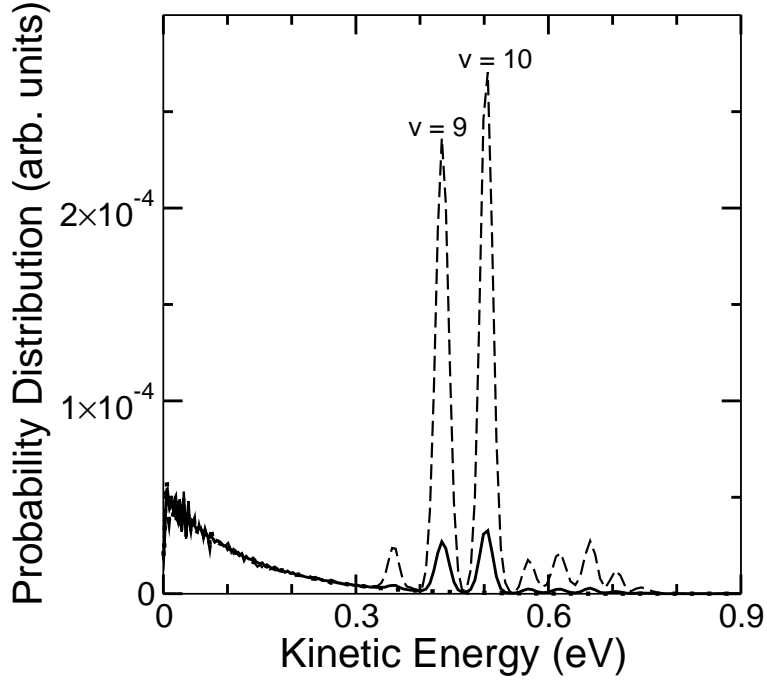


**Figure 3.** Proton energy distribution  $P_k(E_k)$  at low laser intensities. The pulse length is  $T_p = 55$  fs and  $\lambda = 790$  nm. Full line:  $I = 5 \times 10^9 \text{ W cm}^{-2}$ ; dashed line:  $I = 5 \times 10^{10} \text{ W cm}^{-2}$ . The low-energy background (dotted line) is the shake-off spectrum. The vibrational lines are single-photon peaks. The high intensity lines are 10 times stronger than the low intensity results as expected from perturbation theory.

background. This can be achieved by projecting out the continuum or by waiting for the shake-off to occur and absorb the dissociation. In fact, the shake-off background is an imperceptible perturbation to the results at high intensity, as shown in figure 4. In practice, for intensities above  $5 \times 10^{11} \text{ W cm}^{-2}$ , we have not found it necessary to remove the shake-off wavepacket a priori. At higher intensities the two-photon dissociation process becomes important, and in figure 4 (b) we include vertical dotted lines to indicate the expected positions of these peaks. Again, at the highest intensities, the spectrum peaks move towards the lower energies although the spectrum also broadens. The peak heights in figure 4 (c) and (d) are similar, but the yield is much higher for the higher intensity. The corresponding dissociation probabilities  $P_d$  for each intensity are ?????. As mentioned before, increasing the angle between molecule and polarization is equivalent to decreasing the intensity. Then figure 4 represents the angular-differential dissociation rates. Thus for a spatially uniform pulse of cycle-average intensity  $I = 5 \times 10^{14} \text{ W cm}^{-2}$ , figures 4 (b),(c) and (d) are respectively the yields at  $\theta = 72, 84$  and  $88$  degrees. For pulses much longer than the vibrational time, the initial phase of the molecular wavepacket is not a significant factor. Averaging over the initial phase has little effect. In the next section we will consider pulses of duration comparable to the vibrational dephasing time.

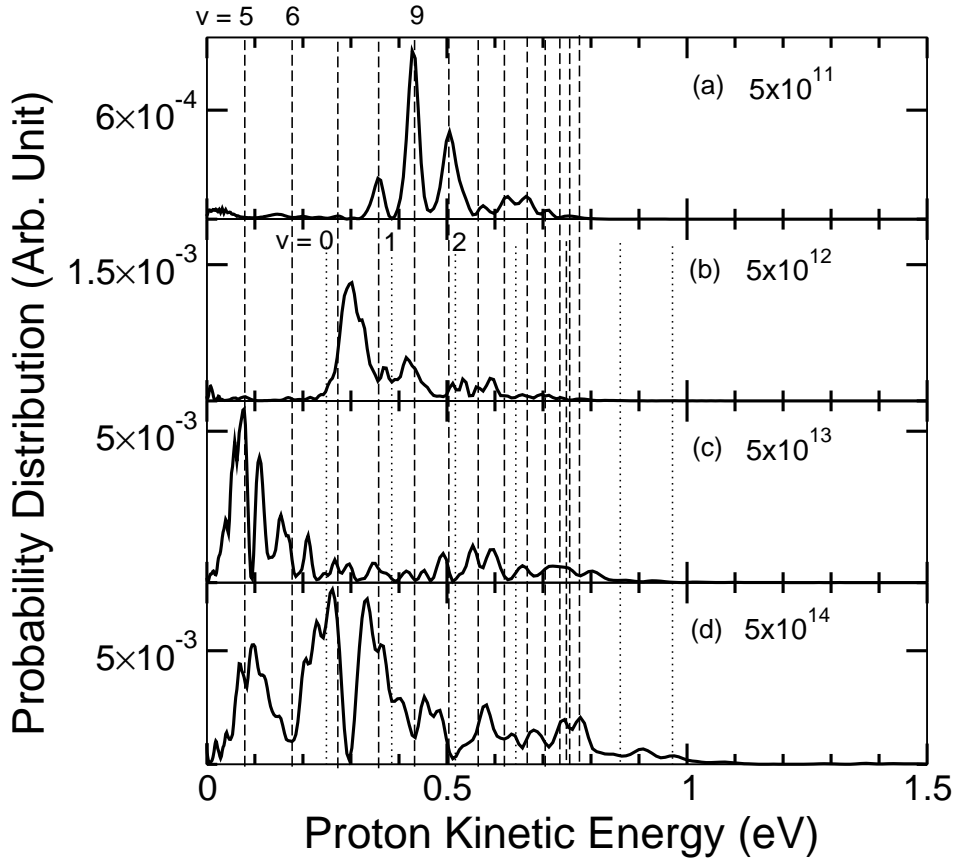


**Figure 4.** Proton energy distribution at different intensities. The initial vibrational wavepacket is prepared from  $H_2$  ( $v = 0$ ). The pulse parameter are  $T_p = 55$  fs and  $\lambda = 790$  nm. The dashed vertical lines indicate the one-photon vibrational release with one photon absorption from different vibrational states and the dotted vertical line show those with two photon absorption.

### 3.3. Vibrational phase and pulse length

In the well-known 'pump and dump' technique, for heavy atoms within a molecule, the vibrational motion can be easily resolved by 100 fs pulses. However for the hydrogen atom the vibration is so fast ( $\sim 15$  fs) that this requires pulses of 40 fs or shorter. We have already shown (figure 2) that for  $H_2^+$ , the vibrational phase has a role for 20 fs or less. In this section we consider the effect on the coherent wavepacket of  $v'$  states created from the  $v = 0$  state, and speculate on whether this can be resolved by experiments measuring the proton emission spectrum. We begin with a study of pulse length effects for the coherent state. In figure (5) the features of the low-intensity pulse are considered for  $\lambda = 790$  nm and  $I = 5 \times 10^{11} \text{ W cm}^{-2}$ , choosing the molecular vibration phases by starting the clock (pulse) at  $t' = 0$ . As noticed previously for  $v' = 0$ , for very short pulses the bandwidth broadening and reduced duration leads to a flat spectrum with low dissociation yield. Increasing the pulse duration allows the vibrational structure to be clearly resolved at  $T_p = 40$  fs and the familiar Franck-Condon distribution highlighted in figure (3) is apparent. Also evident in figure (5) is the interference of the shake-off background with the low-energy spectrum.

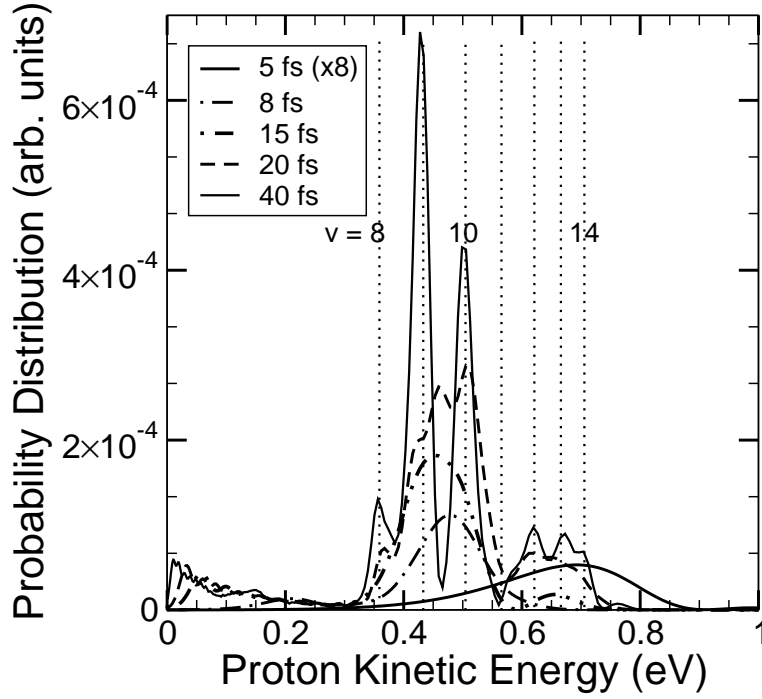


**Figure 5.** Dependence of proton energy distribution on pulse length.  $I = 5 \times 10^{11} \text{ W cm}^{-2}$  and  $\lambda = 790 \text{ nm}$ . The corresponding laser pulse length is indicated in the figure for each curve.

At higher intensity it has been shown that the vibrational signature in the dissociation spectrum can be destroyed to a large extent, even for long pulses. Increasing intensity to  $I = 5 \times 10^{13} \text{ W cm}^{-2}$ , confirms that this occurs for the coherent state (figure 6). Firstly, the proton energies shift to less than 1 eV. We note that for the 40 fs pulse, the data is very similar to the 55 fs pulse shown in figure 4 (c). At the other end of the time scale, for 5 fs pulses, the protons emerge with much higher energies

That is, apart from the broadening of the peak due to bandwidth effects, the wavepacket favours the high frequency part of the pulse. However it is clear that in this case the pulse delay, or molecular phase, has an important role [37, 38] and [39, 40]. In figure (7) we consider the 5 fs pulse and we present results for the wavepacket distribution in space along with the proton energy spectrum. The pulse is delayed by up to 20 fs with respect to the molecular vibration. Firstly examining the energy spectrum, there is clearly a strong variation with pulse delay. The 0.7 eV peak that appears in figure 5 corresponding to the 5 fs peak with time delay 0 fs is clearly present in figure 7. The corresponding state in  $R$ -space is the Gaussian wavepacket centred at  $R = 1.4$ . The short delay time allows the molecule to dissociate from small  $R$  values and accelerate along the  $\Sigma_u$  curve. With a delay of 1 fs the wavepacket moves outwards and disperses, this delay severely decreases the dissociation yield and attenuates the dissociation energy. After 7 fs delay the molecular wavepacket is at the outer turning point. A pulse applied at this time yields a low yield peaked around 0.4 eV. As the delay time increases the vibrational components separate and dephase. At 20 fs for example, the wavepacket is irregular and diffuse as the high  $v'$  components become evident. The dissociation from this wavepacket produces a strong low-energy signal at 0.3 eV.

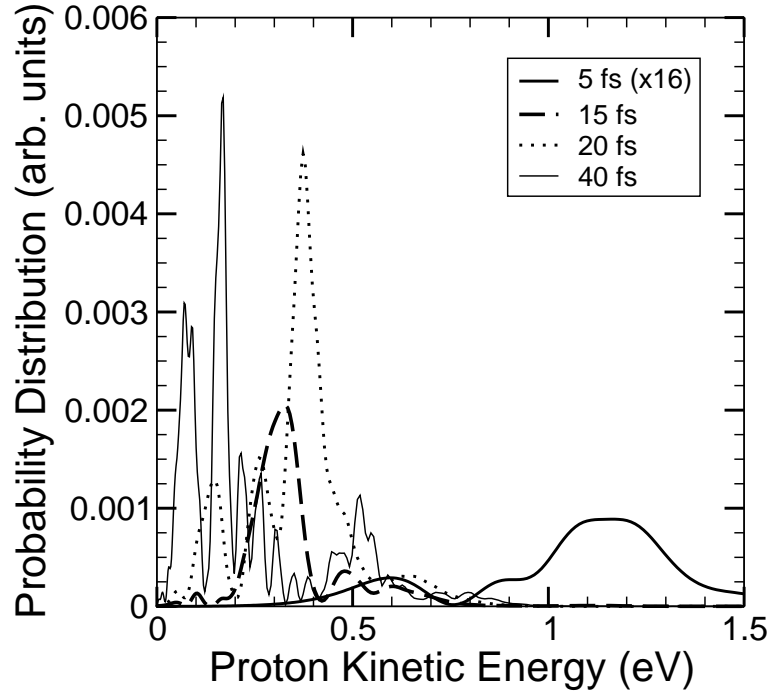


**Figure 6.** Dependence of proton energy distribution on pulse length.  $I = 5 \times 10^{13} \text{ W cm}^{-2}$  and  $\lambda = 790 \text{ nm}$ . The pulse duration is indicated in the figure.

Comparing with figure 4 for example, this energy can only be a bandwidth shifted state. That is, the  $v = 9$  state dissociating through a low energy photon. In a real experiment the random phases of vibration mean that these details are often lost. The molecular phase (clock) can be synchronized by using the same laser for photoionization and dissociation [37, 38]. However, the assumption that primary photoionization of  $H_2$  is a vertical transition has recently been shown to be invalid [14]. This is not too surprising since it is generally not a good assumption for infrared light at high intensity. However it is a reasonable model for UV light or electron impact ionization.

Clearly the sensitivity of the proton spectrum is potentially a very useful tool for experimental diagnostics. The difficulty still exists in that a real laser pulse has temporal and spatial variations that can impede the observation of these details. For a long pulse  $T_p = 40 \text{ fs}$ , our calculations show that the kinetic energy distribution is not sensitive to the time-delay at the same intensity of  $5 \times 10^{11} \text{ W cm}^{-2}$ . At higher intensity of  $5 \times 10^{13} \text{ W cm}^{-2}$ , the spectrum shows only small structure effects due to pulse delay. In order to test our model with experiment we conclude our paper with a study in which we take into account the experimental parameters and integrate over the focal volume of the pulse and average over molecular orientation.

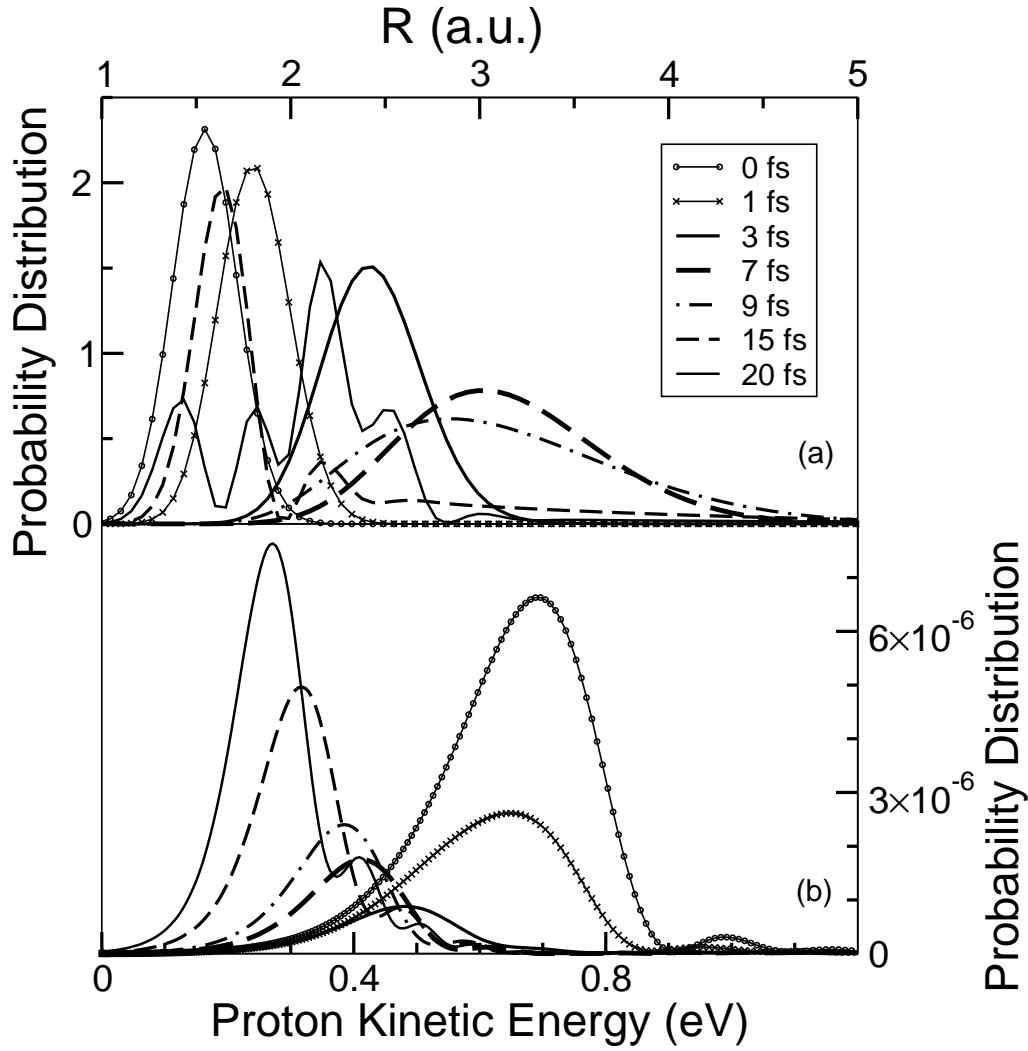


**Figure 7.** Effect of vibration phase (time delay) for 5 fs pulses.  $I = 5 \times 10^{11} \text{ W cm}^{-2}$  and  $\lambda = 790 \text{ nm}$ . (a) The  $R$ -space probability density at the start of the pulse; (b) The corresponding proton energy distribution after the pulse. The different time delays are indicated in frame (a).

### 3.4. Comparison with Experiment

The experiment [10] allows the dissociative and dissociative ionization processes can be discriminated by coincidence time-of-flight measurements. The spectrum can be dominated by the large low intensity focal volume. For a theoretical model the relevant spectrum is the probability distribution given by

$$P(I_f, E_p) = \int \int 2\pi\rho P_k(I(\rho, z), E_k) d\rho dz \quad (29)$$

where  $I_f$  is the peak intensity in the focus center and  $E_p$  is the kinetic energy of the proton. The focus averaging over all these data with the peak intensity  $I_f = 2 \times 10^{15} \text{ W cm}^{-2}$  produce figure 8 which is in excellent agreement with the experiment for the pure dissociation peak [10]. Unfortunately, many of the structures present in the proton energy spectrum are lost after

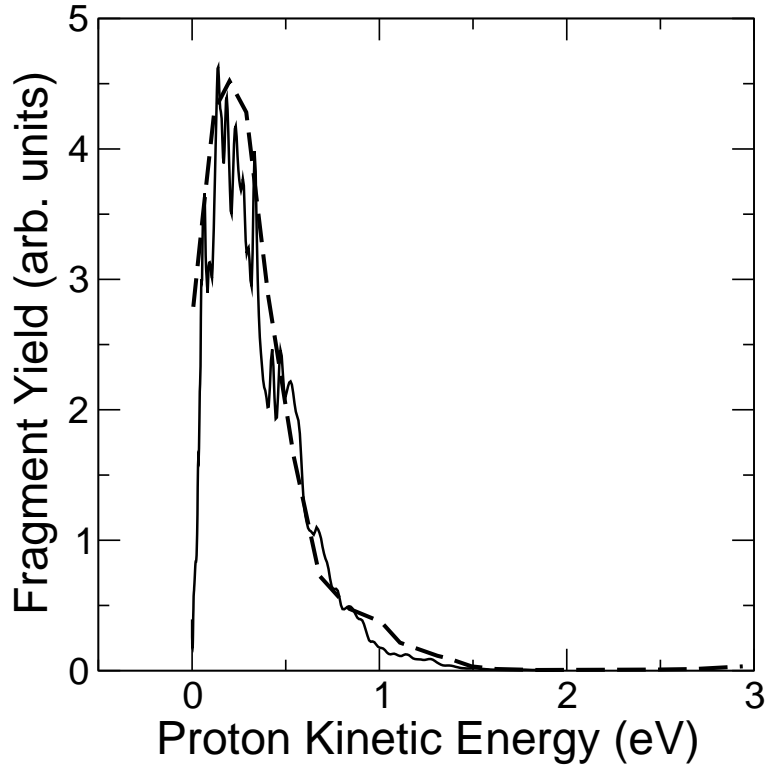


**Figure 8.** Proton energy distributions from theory and experiment.  $I = 3 \times 10^{15} \text{ W cm}^{-2}$  with  $\lambda = 790 \text{ nm}$  and  $T_p = 65 \text{ fs}$ .  $w_0 z_R = .$  Full curve: Present calculation; dashed line: experimental measurement from the pure dissociation channel [10].

the averaging process. The small resonant structures in the theoretical modelling correspond to the dissociation from different vibrational levels. At this intensity, saturation occurs at the centre of the focus, thus a large fraction of the dissociation fragments arise from the outer intensity shells. This is confirmed by our calculation in which the proton spectrum has a similar shape for a peak intensity  $5 \times 10^{14} \text{ W cm}^{-2}$  and  $3 \times 10^{15} \text{ W cm}^{-2}$ . Nonetheless the shape and ion yield of the experiment are extremely well characterised in this experiment, and it is highly encouraging that theory and experiment are in such good agreement. More recent measurement techniques, develop in the last two years, allow sections of the focal volume to be studied, providing and much more detailed examination of the proton spectrum. These new measurements will hopefully reveal some of the features of the proton energy spectrum described in our paper.

#### 4. Conclusions

In summary, we have thoroughly investigated the dissociation dynamics of  $H_2^+$  in strong laser fields. The vibrational-state resolved kinetic energy distributions have been calculated at various intensities ranging from  $5 \times 10^9 \text{ W cm}^{-2}$  to  $3 \times 10^{15} \text{ W cm}^{-2}$  for  $\lambda = 790 \text{ nm}$ . The results show the sensitivity of the kinetic energy distribution on the laser intensity, molecular orientation, the pulse length and the pulse delay. At very high intensity, our focus-averaging

results reproduce the experimental measurements very accurately [10]. Most importantly, we demonstrate that molecular dissociation dynamics at rather low intensity with a short pulse duration would be more suitable to act as a sub-femtosecond molecular clock.

## Acknowledgement

This research is supported by the award of a PhD research studentship from the International Research Centre for Experimental Physics, Queen's University Belfast. This work has also been supported by a grant of computer resources at the Computer Services for Academic Research, University of Manchester, provided by EPSRC to the UK Multiphoton, Electron Collisions and BEC HPC Consortium.

## References

- [1] *Molecules and Clusters in Intense Laser Fields*, edited by Posthumus J H ( Cambridge University Press, Cambridge, 2001).
- [2] Posthumus J H 2004 *Rep. Prog. Phys.* **67** 623.
- [3] Frasinski L J and Codling K 1993 *J. Phys. B* ??????
- [4] Giusti-Suzor A , Mies F H, DiMauro L F, Charron E and Yang B 1995 *J. Phys. B: At. Mol. Opt. Phys.* **28** 309.
- [5] Bucksbaum P H , Zavriyev A , Muller H G, and Schumacher D W 1990 *Phys. Rev. Lett.* **64** 1883.
- [6] Miret-Artés S and Atabek O 1994 *Phys. Rev. A* **49** 1502.
- [7] Ludwig J, Rottke H and Sandner W 1997 *Phys. Rev. A* **56** 2168.
- [8] Nguyen-Dang T T, Abou-Rachid H, Nguyen N A, Mireault N, Lévesque J, Vijayalakshmi K and Chin S L 2003 *Phys. Rev. A* **67** 013405.
- [9] Roudnev V, Esry B D and Ben-Itzhak I 2004 *Phys. Rev. Lett.* **93** 163601.
- [10] I D Williams, McKenna P, Srigengan B, Johnston I M G, Bryan W A, Sanderson J H, El-Zein A, Goodworth T R J, Newell W R, Taday P F and Langley A J 2000 *J. Phys. B: At. Mol. Opt. Phys.* **33** 2743.
- [11] Newell W R, Williams I D and Bryan W A 2003 *Euro. Phys. J. D* **26** 99
- [12] Sändig K, Figger H and Hansch T W 2000 *Phys. Rev. Lett.* **85** 4876.
- [13] Pavičić D, Kiess A, Hänsch T W and Figger H 2003 *Euro. Phys. J. D* **26** 39
- [14] Urbain X, Fabre B, Staicu-Casagrande E M, de Ruette N, Andrianarijaona V M, Jureta J, Posthumus J H, Saenz A, Baldit E and Cornaggia C 2004 *Phys. Rev. Lett.* **92** 163004.
- [15] Dundas D 2002 *Phys. Rev. A* **65** 023408.
- [16] Peng L Y Dundas D, McCann J F, Taylor K T and Williams I D 2003 *J. Phys. B: At. Mol. Opt. Phys.*, **36** L295.
- [17] Peng L Y, McCann J F, Dundas D, Taylor K T and Williams I D 2004 *J. Chem. Phys.*, **120** 10046.
- [18] Taylor K T, Parker J S, Dundas D, Meharg K J, Peng L Y, Doherty B J S and McCann J F 2004 *Physics Scripta*, **T110** 154.
- [19] Dundas D , Meharg K J, McCann J F and Taylor K T 2003 *Euro. Phys. J. D* **26** 51
- [20] Plummer M and McCann J F 1995 *J. Phys. B: At. Mol. Opt. Phys.* **28** L119.
- [21] Giusti-Suzor A and Mies F H 1992 *Phys. Rev. Lett.* **68** 3869.
- [22] Zavriyev A, Bucksbaum P H, Squier J and Saline F 1993 *Phys. Rev. Lett.* **70** 1077.
- [23] Yao G H and Chu S-I 1993 *Phys. Rev. A* **48** 485.
- [24] Frasinski L J, Posthumus J H, Plumridge J, Codling K, Taday P F and Langley A J 1999 *Phys. Rev. Lett.* **83** 3625.
- [25] Bunkin F V and Tugov I I 1973 *Phys. Rev. A* **8** 601.
- [26] Bates D R 1951 *J. Chem. Phys.* **19** 1122.

- [27] Lin J T and Jiang T F 2001 *Phys. Rev. A* **63** 013408.
- [28] Heather R and Metiu H 1987 *J. Chem. Phys.* **86** 5009.
- [29] Baye D and Heenen P-H *J. Phys. A* **19** 2041.
- [30] Keller A 1995 *Phys. Rev. A* **52** 1450.
- [31] Keller A 2003 Private communications.
- [32] Jolicard G and Atabek O 1992 *Phys. Rev. A* **46** 5845.
- [33] Giusti-Suzor A, He X, Atabek O and Mies F H 1990 *Phys. Rev. Lett.* **64** 515.
- [34] Dunn G H 1966 *J. Chem. Phys.* **44** 2592.
- [35] Kondorskiy A and Nakamura H 2002 *Phys. Rev. A* **66** 053412.
- [36] Serov V N, Keller A, Atabek O and Billy N 2003 *Phys. Rev. A* **68** 053401.
- [37] Niikura H, Legare F, Hasbani R, Bandrauk A D, Ivanov M Y, Villeneuve D M and Corkum P B 2002 *Nature* **417** 917.
- [38] Niikura H, Legare F, Hasbani R, Ivanov M Y, Villeneuve D M and Corkum P B 2003 *Nature* **421** 826.
- [39] Tong X M, Zhao Z X, and Lin C D 2003 *Phys. Rev. Lett.* **91** 233203.
- [40] Tong X M and Lin C D 2004 *Int. J. Mod. Phys. B* **18** 1659.
- [41] Huber K P and Herzberg G 1979, *Constants of Diatomic Molecules* (Van Nostrand Reinhold, New York)